SAND2022-10344C

Integrated photonics for trapped ion quantum information experiments at Sandia National Laboratories

Hayden J. McGuinness[a], Michael Gehl[a], Craig G. Hogle[a], Daniel Dominguez[a], William J. Setzer[a], Nick Karl[a], Nick Jaber[a], Justin Schultz[a], Joonhyuk Kwon[a], Meagan Ivory[a], Rex R. Kay[a], Matt Eichenfield[a], and Dan L. Stick[a]

[a]Sandia National Laboratories, 1515 Eubank Blvd SE, Albuquerque, NM

ABSTRACT

As trapped ion systems add more ions to allow for increasingly sophisticated quantum processing and sensing capabilities, the traditional optical-mechanical laboratory infrastructure that make such systems possible are in some cases the limiting factor in further growth of the systems. One promising solution is to integrate as many, if not all, optical components such as waveguides and gratings, single-photon detectors, and high extinction ratio optical switches/modulators either into ion traps themselves or into auxiliary devices that can be easily integrated with ion traps. Here we report on recent efforts at Sandia National Laboratories to include integrated photonics in our surface ion trap platforms.

Keywords: Integrated Photonics, Quantum Information, Quantum Sensing, Trapped ions

1. INTRODUCTION

Trapped ion experiments have produced impressive results in the field of quantum information processing.[1–3] Manipulating trapped ions of any species requires several different optical frequency lasers for cooling, state preparation, probing, and detecting the quantum state of the ion, making optical components very important to trapped ion systems.[4] Of the several methods used to trap ions, surface ion traps, two-dimensional, planar, microfabricated devices that use a combination of DC and RF electric fields to trap and transport ions between trap regions, have gained a central role in trapped ion science since their debut.[5,6]

Surface ion traps have become increasingly widespread owing to their potential for precision feature engineering, repeatability, compactness, and ease of use. Within the last several years the possibility of including integrated optical components directly into surface traps has lead to a number of experiments which may point toward a solution to the problem of qubit number scaling. As trapped ion experiments become more ambitious and require higher numbers of ions the traditional optomechanical methods for delivering light (bulk lenses mounted on multi-axis stages), detecting ion light (large objectives outside the chamber funneling light to macroscopic detectors), and modulating light (arrays of individual acousto and electro-optical AO/EO modulators), become increasingly infeasible due to their tendency for misalignment and fragility. Integrated photonic technologies are well suited for surface ion traps and are an intriguing answer to these current limitations.

At Sandia National Laboratories we are working to push forward integrated photonics on surface traps primarily through two projects. One focuses on creating a compact physics package for an optical atomic clock and employs waveguides and gratings to deliver light to ions while also detecting ion fluorescence through integrated single-photon detectors while the other combines waveguide delivery integrated optical modulators for fast optical switching. We report on recent accomplishments and ongoing efforts towards integrated optical components and surface ion traps.

Author to whom correspondence should be addressed: hmcgui@sandia.gov

2. INTEGRATED OPTICAL WAVEGUIDES, GRATINGS, AND PHASE SHIFTERS

Continued scaling of surface ion traps to larger numbers of trapped ions will require new solutions to the delivery and collection of light.[7–9] This becomes even more critical as traps move to two-dimensional arrays of ions, limiting optical access from the side. We're addressing this challenge through the integration of optical waveguides into the dielectric below the electrodes of the ion trap. Efficient delivery of the light from an optical fiber to the ion location requires low loss coupling from the fiber into the integrated waveguide, low loss propagation and routing through the trap and finally efficient scattering of the light to a small radius spot at the ion location.

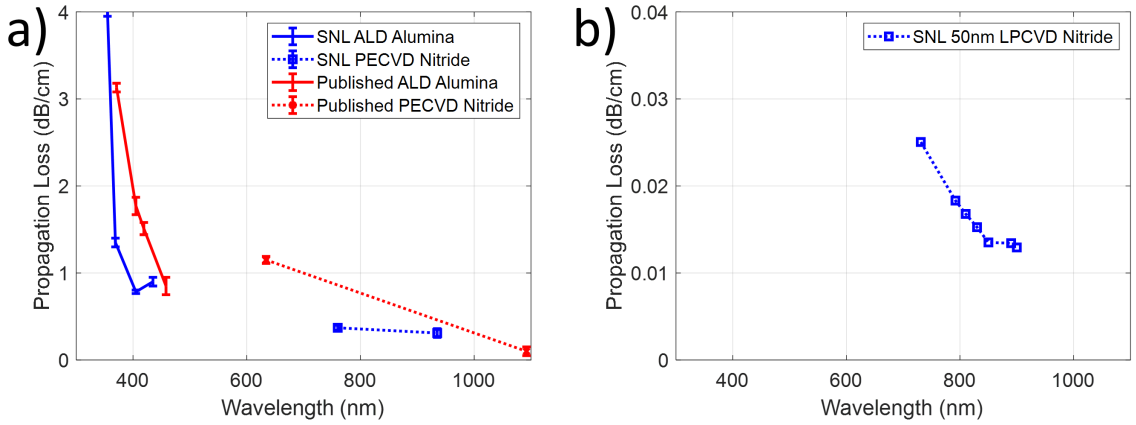

Figure 1. a) Measured propagation loss of Sandia's high confinement aluminum oxide and PECVD silicon nitride waveguides compared to the literature[10] and b) propagation loss of low confinement LPCVD silicon nitride waveguides.

To achieve state-of-the-art propagation loss, we have optimized the materials and fabrication of our waveguides specifically for UV to NIR wavelengths. For wavelengths in the range of ∼500 nm to 1000 nm we have developed a low loss CMOS compatible nitride film and have demonstrated losses on the order of 0.2 to 0.3 dB/cm in the NIR wavelength range. For wavelengths below 500 nm, we have developed an atomic layer deposited (ALD) aluminum oxide film with losses below those reported in the literature.[10] We observe waveguide loss below 1 dB/cm at 400 nm and 1.3 dB/cm at 369 nm. Figure 1 a) plots these various results. These waveguides are intentionally designed to provide high confinement of the optical mode. This reduces the size of the optical mode and also reduces the minimum allowable bend radius, providing compact and simple routing of optical waveguides between the multiple metal layers of our surface ion traps. However, this waveguide geometry is not particularly optimal for reducing optical losses and further improvements in loss can be achieved by reducing the thickness of the waveguide material (at the expense of increasing separation between metal routing layers). This reduces material absorption by reducing the overlap of the mode with the waveguide material (SiN or Al_2O_3). It also reduces the area of the sidewalls which are responsible for a majority of the scattering loss due to etch roughness. As an example of the improvement that is possible, Figure 1 b) shows the propagation loss of a 50 nm thick LPCVD silicon nitride film at NIR wavelengths, showing a nearly 100x reduction in loss.

Once on-chip, the light is divided to multiple paths utilizing multi-mode interference (MMI) splitters. Each path is routed to an ion location before the light is finally delivered to the ion using a diffractive grating element. Figure 2 a) shows a SEM image of one of these MMI splitters, along with two gratings positioned around the location of one of the ion loading holes. The gratings are designed to scatter light at a specified angle and focus to a specified spot diameter at the location of the ion. Figure 2 b) shows an example of the diffracted light profile at the plane of the grating (0 μm) at the plane of the intended focus (50 μm) and above the focus plane (100 μm). In this case, the focused spot size is roughly 4 μm full width half maximum. Due to the limitations on the overall size of the grating and the minimum dimension achievable by photolithography, we typically observed efficiencies on the order of 25 %,[9] however, higher efficiency is possible utilizing electron beam lithography,[7] bottom reflectors and more complex grating designs.[11] In Figure 2 c) we show the measured diffraction angle of a set of 8 nominally identical gratings spread across a distance of more than 6 mm on a single die. We find that we're able to hit the targeted angle of diffraction within 0.5° and we find excellent uniformity with the angle deviating by only ±0.1° or roughly ±185 nm spatial shift at the location of the ion.

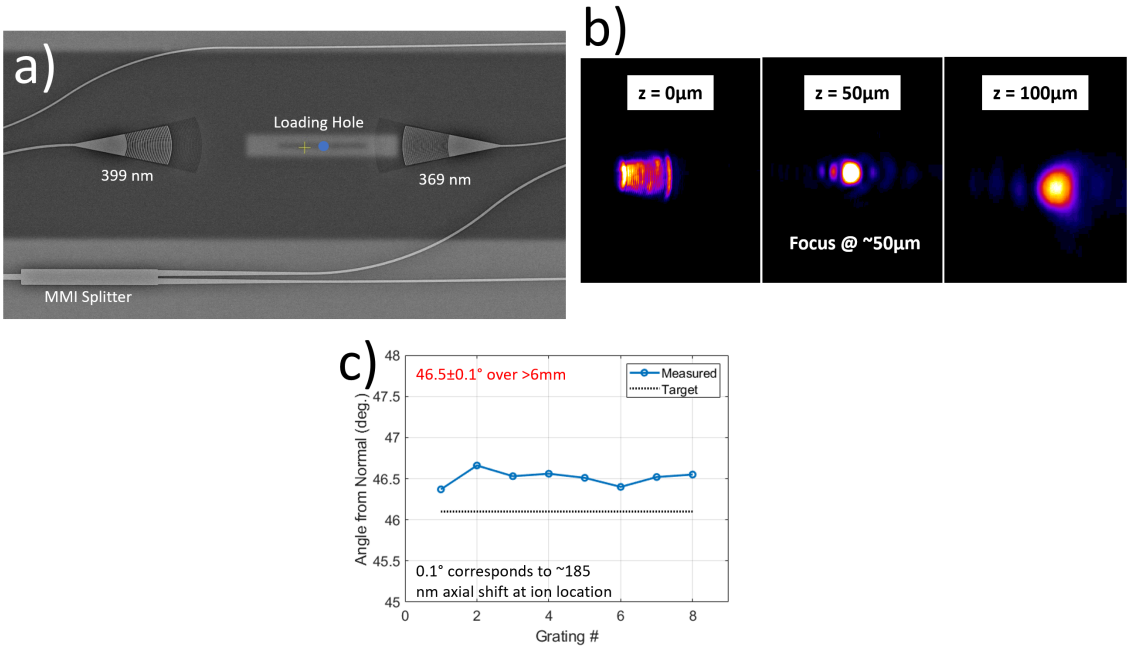

Figure 2. a) SEM image of aluminum oxide MMI splitter and two gratings surrounding an ion loading hole and b) measured diffracted light profile at three heights above the surface of the ion trap. c) Measurement of 8 gratings spread across a distance of more then 6mm, showing our ability to hit the targeted diffraction angle within 0.5° and demonstrating high uniformity.

Active control of light on chip is a desirable feature for controlling relative amplitude, phase and polarization before delivery to trapped ions. In section 4 we describe a technique for high-speed modulation. For lower speed operations, thermal phase shifters can provide low loss and compact optical control. We have demonstrated a high efficiency thermal phase shifter utilizing thermal isolation of the waveguide. Figure 3 b) shows images of the phase shifter which consists of a straight waveguide section ($\sim 240\mu m$ in length) alongside a resistive metal heater. Thermal isolation trenches are etched through the silicon oxide on each side of the structure, and the silicon substrate is etched away directly below the heater. In Figure 3 a) we show the optical transmission through a Mach-Zehnder interferometer as the phase of one arm is swept using one of these phase shifters. We see that it takes approximately 13.3 mW of electrical power to shift the phase by 2π. We also observe 30 dB of extinction, an indication of the high performance of the MMI splitters used to split and recombine the light.

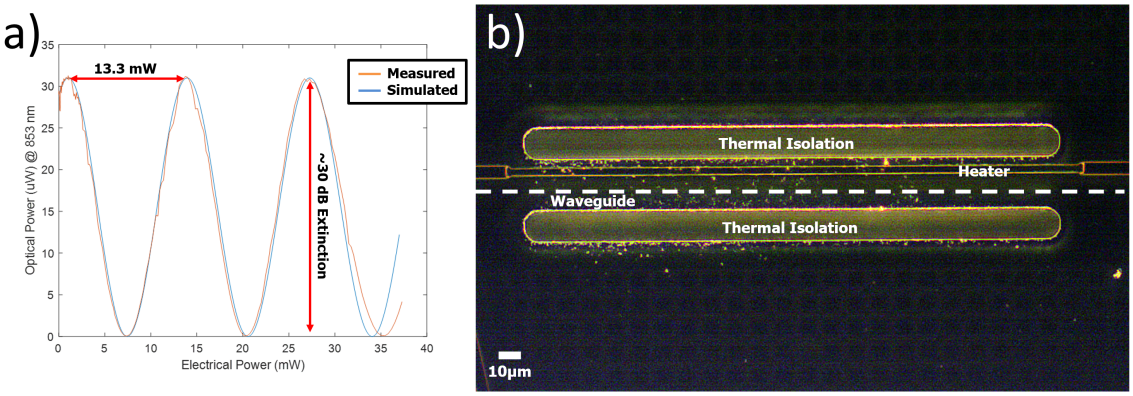

Figure 3. a) Measured intensity through a waveguide integrated Mach-Zehnder interferometer using a high efficiency thermo-optic phase shifter and b) dark field image of the thermally isolated thermo-optic phase shifter.

We have successfully trapped in several waveguide integrated traps recently and demonstrated high fidelity

quantum control with $^{171}Yb^{+}$ ions. Figure 4 a) shows heating rate measurements as a function of position for a trap containing waveguides and gratings that supported 435 nm light delivery.[9] All positions of the ion, from the loading location, to the region where waveguide light was incident upon the ion at a ~ 45 degree angle, to directly above the grating showed similar heating rates. Notably, the layer of oxide which covers the output gratings and was exposed to the ion through an aperture cut into the top metal of the trap, did not cause significant heating. This is surprising in that exposed dielectric often collects charge, which perturbs the ion, leading to ion heating. Additionally, as seen in Figure 4 b), we achieved relatively coherent Rabi flopping on the ion's blue side band with waveguide delivered light, leading us to measure an average temperature after sideband cooling of $\bar{n} = 0.1$. As of time of writing we have demonstrated trapping with only waveguide delivered light using 369 and 935 nm beams but have yet to measure heating rates or show quantum control operations with waveguide light with this trap.

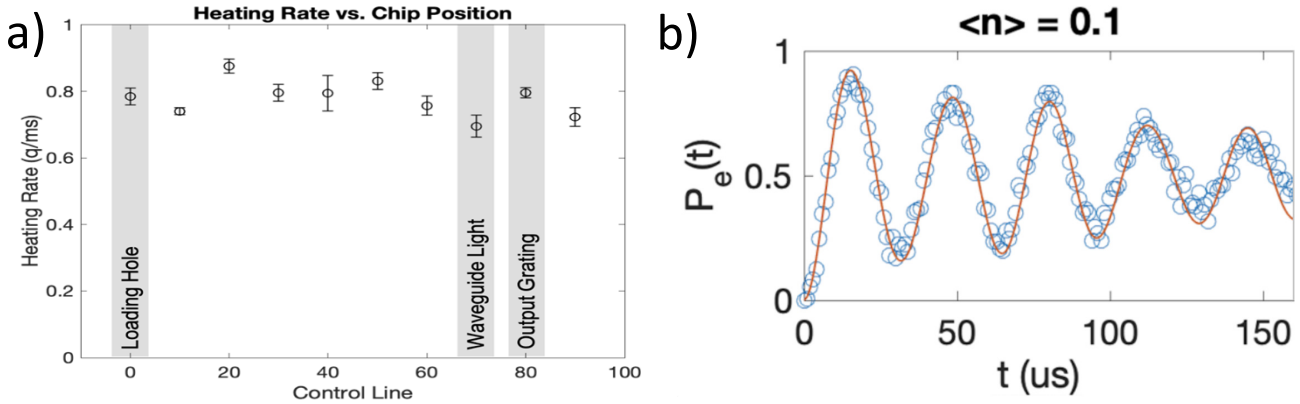

Figure 4. a) Heating rate measurements as a function of trap position. There was relatively little difference in rate, even near the output grating which exposed dielectric to the ion. b) Rabi flopping on the ion's blue sideband. The average temperature after sideband cooling was $\bar{n} = 0.1$.

3. SINGLE-PHOTON AVALANCHE DETECTORS

Another crucial task for trapped ion experiments is detecting the quantum state of ions. This is generally accomplished through fluorescence detection, with the ion fluorescence captured with an objective external to the vacuum chamber and sent to a photomultiplier tube (PMT) or single-photon avalanche detector (SPAD) which counts the number of collected photons in a given detection window. There are many advantages to this setup, such as ease of optical alignment, the ability to swap components, cost, and overall ease of use. Similar to free-space optics for beam delivery, a major disadvantage to external detection systems is that it would be challenging for external objectives and detectors to efficiently manage a system composted of thousands or millions of ions.[12] Other disadvantages revolve around the large size, weight, and power (SWaP) and fragility of these systems, making them unsuitable for systems requiring a compact form factor or ability to function in dynamic environments. Efforts have been made to place collection optics inside the chamber and near or on the trap to address these issues including optical fiber,[13] micro-fabricated optics,[14] optical cavities,[15] and more. In 2020 a superconducting nanowire single photon detector (SNSPD) was monolithically fabricated into an ion trap and demonstrated UV detection of a $^{9}Be^{+}$ ion,[16] the first demonstration of a trap-integrated single photon detector.

Recently we demonstrated the first surface trap integrated SPAD with a $^{174}Yb^{+}$ ion operating at room temperature and having a single-photon detection efficiency at the detection wavelength of 370 nm of 24%.[17] Other demonstrations of SPAD-integrated surface traps soon followed.[18] Figure 5 a) shows the surface trap and array of integrated SPADs, with the inset showing a close-up image of one SPAD. Ions are loaded into the trap by ionizing Ytterbium atoms incident on the back side of the trap and pass through small slots that run through the wafer and allow access to the front side of the trap. Once trapped with RF and DC electric fields, the ions

can be moved ("transported") along the length of the trap by varying the voltages of the DC fields. This allows for ion transport close to, or even directly over, the SPADs.

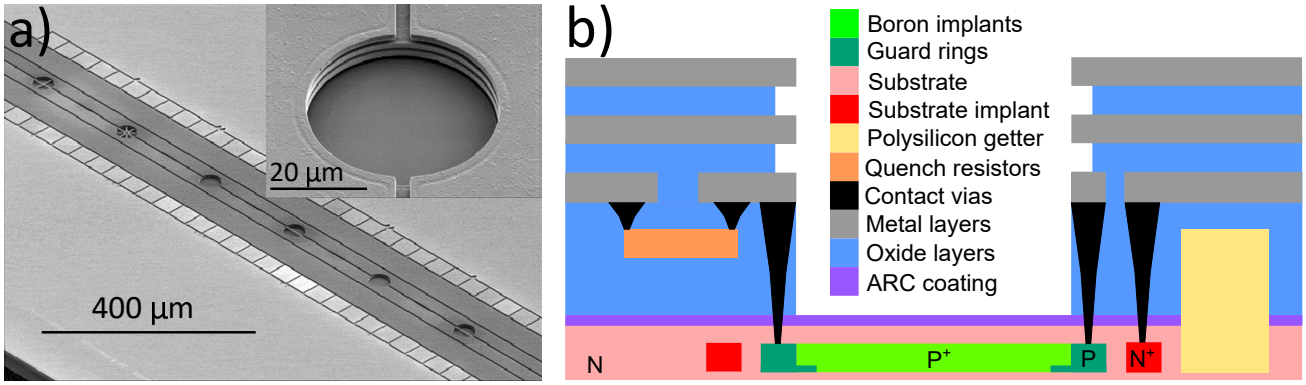

Figure 5. a) SEM images of the surface trap with an array of SPADs. The outside squares are the DC electrodes which provide some of the ion confining potential, the other part of the potential is generated by the RF rails just inside the DC electrodes. Some of the SPADs have grounded metal covers which are designed to provide some protection for the ion from the perturbative electric field generated when the SPADs fire. b) Cartoon cross-section, not-to-scale, of SPAD geometry and composition .

Figure 5 b) shows a cartoon cross-section of the SPAD/surface trap device. A 5 μm thick layer of N-doped silicon, common to all SPADs on the trap device, serves as the cathode. The optically sensitive area, the anode, of the SPAD is created by implanting a high concentration of Boron in the N-doped silicon. To control the edge breakdown in the SPADs, an area around the anode is implanted with a lower concentration of Boron called the "guard ring".[19] This guard ring reduces the electric field at the anode boundary, which ensures the highest electric field and hence highest charge multiplication region, is in the the central bulk region of the device rather than at the edges and surface. To reduce photon reflection, an anti-reflection coating of silicon dioxide and silicon nitride with total thickness of $\sim$ 40 nm is deposited on the SPAD surface. To bias the substrate as well as collect the current from a detection event, tungsten contact vias connect the SPAD layers to the first trap metal layer. Polysilicon quench resistors with values of roughly 300kΩ debias the anode after the SPAD fires. Because the resistors are integrated with the SPAD, the total capacitance that must be discharged through the SPAD when fired and re-charged through the resistor is minimized. This result in lower cross-talk, after-pulsing, and dead time. The entire SPAD fabrication process flow could be ported to most industrial CMOS foundries. To mitigate dark counts, caused by thermally generated carriers,[20] each SPAD area is split into either quarters or halves, effectively making multiple detectors at each $\sim$ 38 μm diameter SPAD site.

In general, the ions were significantly influenced by the SPADs operation. This was likely due to the electric field caused by the very fast (several nanoseconds) voltage spike that occurs when a SPAD is triggered either by an incoming photon or thermal carriers. The strength of this perturbation overcame the trapping potential when the ion was 68 μm or closer to the center of the quartered SPAD. In this region the ion was quickly lost when the SPADs were operational. So as to operate continuously without significant ion loss, we placed the ion 80 μm from the center of the SPAD for data collection. As mitigation for the detrimental effects SPAD firing has upon the ion, a thin film of conductive but transparent indium tin oxide (ITO) patterned directly on top of the SPAD or a metal "mesh" cover patterned on one of the metal layers above the SPAD could be used to drastically reduce the influence of SPAD firing on the ion while allowing a majority of the ion fluorescence to be incident upon the SPAD. At time of writing we currently have under test a surface trap employing a metal mesh, connected to the ground plane metal layer, which allows $\sim$ 56 % of ion fluorescence to fall upon the SPAD and is shown in Figure 6 a). Qualitatively, this mesh allows for the SPAD to operate while the ion is stably positioned directly above the SPAD. Future work on this trap will include using $^{171}Yb^{+}$ ions, enabling coherence time and heating rate measurements.

We investigated the performance of a quartered SPAD having an area of roughly 60 μm^2 for a SPAD with no metal cover as shown in Figure 5 a). At an overbias above breakdown of roughly 1.5 volts this SPAD's dark

counts were 1.2 kcps. This overbias voltage level presented a good trade-off between detection efficiency and dark count rate. Covering the SPAD was an anti-reflective coating (ARC) designed to minimize reflection off the high index silicon surface when light is normally incident upon the surface. Due to the inability of the trap to hold an ion directly over the SPAD when the SPAD is operational, the angle of incidence was large, over 45 degrees, and the ARC coating was only partially effective. We estimate a reflection of 370 nm from 17% to 23%, depending on the location of the ion. A further effect of the high incidence angle, and small quartered SPAD area, is that the total fluorescence collection efficiency at 80 μm away from the SPAD center was only 0.03 %. To maximize counts and efficiently cool the ion, we set our detection beam intensity to 83 % of the transition's saturation intensity.

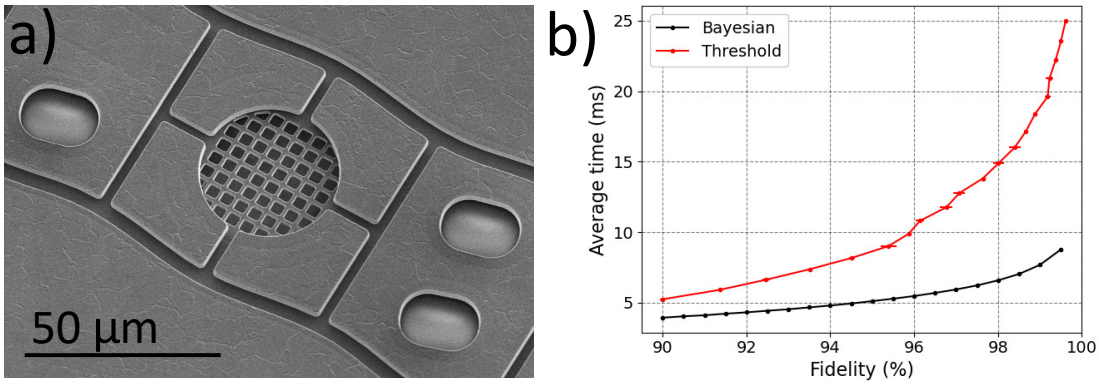

Figure 6. a) SEM image of surface trap having circular SPADs with grounded metal mesh cover. The surrounding slots allow output gratings to deliver light directly over the SPAD. These apertures cut through the DC electrodes. b) Mean time for detection as a function of fidelity for the Bayesian and standard threshold methods. The Bayesian method offers faster detection times at the cost of increased computational complexity.

We characterize the performance of the SPAD by collecting count data with the ion present and not present in the trap. In order to explore relative advantages of different measurement analysis techniques we collected the digitized, timestamped SPAD output over the course of 50 seconds with and then without an ion in the trap. Detection fidelity of the ion/no ion timestamped data was calculated using the standard "threshold" technique, employing a set detection gate time, and with an adaptive Bayesian technique which implemented a variable detection gate time to achieve a target fidelity.[21] The results are shown in Figure 6 b), with the Bayesian method being from a factor of two to three times faster than the standard threshold method given a particular target fidelity. The clear advantage in quick detection time the Bayesian technique exhibits is somewhat mitigated by the additional computational resources it requires as compared to the threshold method.

4. MODULATORS

Integrated waveguides/gratings and detectors potentially solve some of the significant problems with scaling trapped ion, or any optics-dependent, quantum information systems. However, the delivered light must still be manipulated in at least amplitude and phase, and possibly frequency, at the individual ion level. For systems with a small number of ions this is accomplished off chip, and usually out of chamber, by the use of AOMs and EOMs. For future systems having large numbers of ions this solution is not tenable.

One solution is to integrate optical modulation into the waveguide delivery system, either by co-fabricating them with a surface trap or fabricating a separate modulator device which then is coupled to a waveguide integrated surface trap. Light of a power sufficient to drive multiple ions could be coupled into a waveguide at which point the light is fanned out into several channels with MMI splitters, with each channel having their own integrated modulator, and then be incident on individual ions after a grating outcoupler. While each modulator requires at least one electrical control signal for operation, the problem of electrical I/O is less challenging than that of optical I/O. Electrical input via wire bonding can achieve greater density, and is easier to implement

than optical input via edge or grating coupling.[22] For the greatest potential scalability, the modulators ideally would be fabricated in a CMOS-compatible process.

Using integrated Mach–Zehnder interferometers (MZIs), on a seperate device from our surface traps, we've carried out a proof-of-principle experiment demonstrating single-qubit operations on trapped $^{40}Ca^{+}$ ions on the $S_{1/2}$ to $D_{5/2}$ at a wavelength of 729 nm. These MZIs are balanced, having two input and two output ports, two waveguide arm sections, and is actuated via a piezo-optomechanical mechanism that changes the optical path length in each arm with applied voltage.[23*] This is accomplished by situating the curving waveguide arms on top of a piezoelectric substrate, which in turn is attached to the underlying wafer through a rectangular support running the full length of the arm. When voltage is applied to the piezo platform it deforms by either expanding or contracting, changing the geometry of the waveguide and hence its path length and relative phase. The MZI is designed so that the two arms are actuated by different voltage sources, which when chosen such that one arm expands and the other contracts, the relative phase difference is enhanced. Two MZIs in serial, shown in Figure 7 a), were used in the experiment for better extinction.

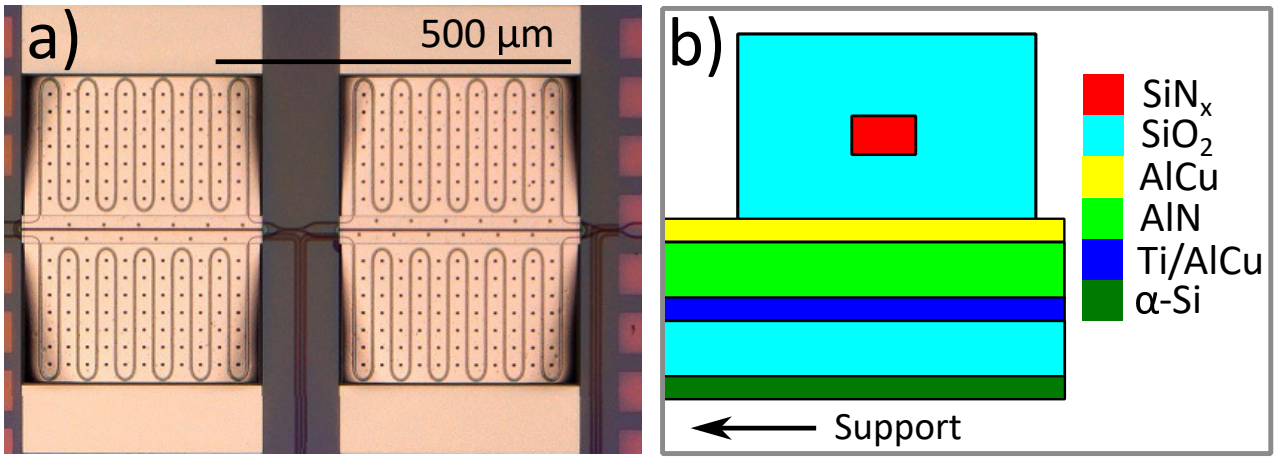

Figure 7. a) An optical image of the two MZIs in serial used for the GST experiments. The input, intermediate, and output MMI can be seen on the far left, middle, and far right. b) Cartoon cross-section of the waveguide structure atop the piezo platform near the outer edge of the platform. The majority of the platform is undercut to allow for deformation when actuated, with the support connecting the platform to the wafer at the middle of the platform.

Power is input into the MZI arms via a 50:50, 1 x 2 MMI. After traveling through the two arms and accumulating some relative phase offset determined by the two voltages applied to the piezo platform arms, the two arms are combined through the inputs of a 50:50, 2 x 2 MMI, with the power in each output port determined by the relative phase differences of the two arms. The MZIs used for the trapped ion experiment had arms with optical path lengths of approximately 1.9 mm. As shown in the not-to-scale Figure 7 b), the waveguide core, SiN_x, was a rectangle 0.285 x 0.4 μm^2, slightly off-center in an oxide rectangle. The voltage required to produce a π phase shift was 24 volts in each arm, with switching times of around 750 ns. An extinction ratio for the two MZIs in serial of 38 dB was achieved.

As of time of writing we have obtained preliminary results using the MZI as an inline on/off switch while performing single-qubit Gate Set Tomography (GST) on trapped $^{40}Ca^{+}$ ions. GST is a protocol for characterizing logical gates for quantum information systems, and offers advantages over other characterization techniques by being calibration free and characterizing all operations in a given gate set simultaneously and self-consistently.[24] Here the gate sets consisted of various combinations of G_x,G_Y, and G_I single-qubit gates. The time it takes when the probe beam is on to transition from one state to the other, the π time, was 12 μs. Table 4 shows the resulting process infidelity at 95 % confidence for GST with 1) the MZIs inline as the on/off switching mechanism with the input power stabilized before the MZIs, 2) using traditional AOM switching with input to the AOMs

*This approach can accommodate a large wavelength range as it doesn't depend on frequency-resonant structures to operate.

stabilized, and 3) AOM switching but with the power was stabilized after passing through the experiment. For the MZI experiment, a double-pass AOM was used to switch between frequencies to accomplish quantum state preparation and probing but was not used to turn the beam on and off. The results for the MZIs and AOMs with input stabilization are fairly similar for the G_x and G_Y gates, showing that while the probe is turned on the MZIs don't impact the probe light's spectral properties, with the overall performance difference likely due to the worse extinction ratio exhibited by the MZIs. For the G_I identity gate, which aims to not change the state at all by ideally shinning no probe light on the ion, the results were noticeably worse. Similar to the G_x and G_Y gates, this is likely due to the worse extinction ratio of the MZIs with the effect enhanced since the time the probe needs to be turned off is longer for G_I gate experiments than for G_x and G_Y gate experiments. Unsurprisingly, the post-chamber power stabilization with AOM switching yields the best performance since this method can account for nearly all power fluctuation throughout the entire experimental apparatus. As of yet we have not implemented the feedback mechanism on the MZI switch to allow for this type of stabilization, which should improve results, will be implemented in future experiments.

Switch	G_x	G_y	G_I
MZI, before	0.0026	0.0024	0.0026.
AOM, before	0.0016	0.0015	0.0007.
AOM, after	0.0007	0.0010	0.0001.

Table 1. Process infidelities of single-qubit G_x, G_y, and G_I gates characterized with GST using different on/off switching mechanisms. The terms "before" and "after" refer to the probe power being stabilized either before entering the switch or after the probe has passed through the chamber.

5. CONCLUSION

As trapped ion systems move towards using higher number of ions and ever increase complexity the need for scalable system architecture is more important than ever. Key to scalablity for trappped ion system is the miniaturization and ruggedization of optical components. We have demonstrated several important photonic technologies that have been integrated into surface ion traps, and these proof-of-principle experiments are helping to lead the way to more capable quantum information processing systems.

ACKNOWLEDGMENTS

The authors thank the members of Sandia's Microsystems and Engineering Sciences Application (MESA) facility for their fabrication expertise and for helpful comments on the manuscript. This work was supported by the Defense Advanced Research Projects Activity (DARPA) and the Department of Energy (DOE). Sandia National Laboratories is a multi-mission laboratory managed and operated by National Technology and Engineering Solutions of Sandia, LLC, a wholly owned subsidiary of Honeywell International Inc., for the U.S. Department of Energy's National Nuclear Security Administration under Contract No. DE- NA0003525. This paper describes objective technical results and analysis. Any subjective views or opinions that might be expressed in the paper do not necessarily represent the views of the U.S. Department of Energy or the United States Government.

REFERENCES

[1] Home, J. P., Hanneke, D., Jost, J. D., Amini, J. M., Leibfried, D., and Wineland, D. J., "Complete methods set for scalable ion trap quantum information processing," *Science* **325**(5945), 1227–1230 (2009).

[2] Harty, T. P., Allcock, D. T. C., Ballance, C. J., Guidoni, L., Janacek, H. A., Linke, N. M., Stacey, D. N., and Lucas, D. M., "High-fidelity preparation, gates, memory, and readout of a trapped-ion quantum," *Phys. Rev. Lett.* **113**, 220501 (2014).

[3] Ballance, C. J., Harty, T. P., Linke, N. M., Sepiol, M. A., and Lucas, D. M., "High-fidelity quantum logic gates using trapped-ion hyperfine qubits," *Phys. Rev. Lett.* **117**, 060504 (2016).

[4] D. J. Wineland, C. Monroe, W. M. I. D. L. B. E. K. and Meekhof, D. M., "Experimental issues in coherent quantum-state manipulation of trapped atomic ions," *J. Res. Nat. Inst. Stand. Technol.* **103**(3), 259–328 (1998).

[5] Stick, D., Hensinger, W. K., Olmschenk, S., Madsen, M., Schwab, K., and Monroe, C., "Ion trap in a semiconductor chip," *Nat. Phys.* **2**, 36–39 (2005).

[6] Seidelin, S., Chiaverini, J., Reichle, R., Bollinger, J. J., Leibfried, D., Britton, J., Wesenberg, J. H., Blakestad, R. B., Epstein, R. J., Hume, D. B., Itano, W. M., Jost, J. D., Langer, C., Ozeri, R., Shiga, N., and Wineland, D. J., "Microfabricated surface-electrode ion trap for scalable quantum information processing," *Phys. Rev. Lett.* **96**, 253003 (Jun 2006).

[7] Mehta, K. K., Zhang, C., Malinowski, M., Nguyen, T.-L., Stadler, M., and Home, J. P., "Integrated optical multi-ion quantum logic," *Nature* **586**(7830), 533–537 (2020).

[8] Niffenegger, R. J., Stuart, J., Sorace-Agaskar, C., Kharas, D., Bramhavar, S., Bruzewicz, C. D., Loh, W., Maxson, R. T., McConnell, R., Reens, D., et al., "Integrated multi-wavelength control of an ion qubit," *Nature* **586**(7830), 538–542 (2020).

[9] Ivory, M., Setzer, W., Karl, N., McGuinness, H., DeRose, C., Blain, M., Stick, D., Gehl, M., and Parazzoli, L., "Integrated optical addressing of a trapped ytterbium ion," *Physical Review X* **11**(4), 041033 (2021).

[10] Sorace-Agaskar, C., Kharas, D., Yegnanarayanan, S., Maxson, R. T., West, G. N., Loh, W., Bramhavar, S., Ram, R. J., Chiaverini, J., Sage, J., et al., "Versatile silicon nitride and alumina integrated photonic platforms for the ultraviolet to short-wave infrared," *IEEE Journal of Selected Topics in Quantum Electronics* **25**(5), 1–15 (2019).

[11] Bramhavar, S., Sorace-Agaskar, C., Kharas, D., Loh, W., Maxson, R., West, G. N., Niffenegger, R., Juodawlkis, P. W., Chiaverini, J., and Sage, J. M., "A visible-light integrated photonic platform for atomic systems," in [*Integrated Optics: Devices, Materials, and Technologies XXIII*], **10921**, 172–176, SPIE (2019).

[12] Kielpinski, D., Monroe, C., and Wineland, D. J., "Architecture for a large-scale ion-trap quantum computer," *Nature* **417**, 709–711 (June 2002).

[13] Clark, C. R., Chou, C.-w., Ellis, A. R., Hunker, J., Kemme, S. A., Maunz, P., Tabakov, B., Tigges, C., and Stick, D. L., "Characterization of fluorescence collection optics integrated with a microfabricated surface electrode ion trap," *Phys. Rev. Applied* **1**, 024004 (Mar 2014).

[14] Merrill, J. T., Volin, C., Landgren, D., Amini, J. M., Wright, K., Doret, S. C., Pai, C.-S., Hayden, H., Killian, T., Faircloth, D., Brown, K. R., Harter, A. W., and Slusher, R. E., "Demonstration of integrated microscale optics in surface-electrode ion traps," *New Journal of Physics* **13**, 103005 (Oct. 2011).

[15] Sterk, J. D., Luo, L., Manning, T. A., Maunz, P., and Monroe, C., "Photon collection from a trapped ion-cavity system," *Phys. Rev. A* **85**, 062308 (Jun 2012).

[16] Todaro, S. L., Verma, V. B., McCormick, K. C., Allcock, D. T. C., Mirin, R. P., Wineland, D. J., Nam, S. W., Wilson, A. C., Leibfried, D., and Slichter, D. H., "State readout of a trapped ion qubit using a trap-integrated superconducting photon detector," *Phys. Rev. Lett.* **126**, 010501 (Jan 2021).

[17] Setzer, W. J., Ivory, M., Slobodyan, O., Wall, J. W. V. D., Parazzoli, L. P., Stick, D., Gehl, M., Blain, M. G., Kay, R. R., and McGuinness, H. J., "Fluorescence detection of a trapped ion with a monolithically integrated single-photon-counting avalanche diode," *Appl. Phys. Lett.* **119**, 1540021 (2021).

[18] Reens, D., Collins, M., Ciampi, J., Kharas, D., Aull, B. F., Donlon, K., Bruzewicz, C. D., Felton, B., Stuart, J., Niffenegger, R. J., Rich, P., Braje, D., Ryu, K. K., Chiaverini, J., and McConnell, R., "High-fidelity ion state detection using trap-integrated avalanche photodiodes," (2022).

[19] Ghioni, M., Gulinatti, A., Rech, I., Zappa, F., and Cova, S. *IEEE J. Sel. Top. Quantum Electron.* **13**(4), 852–862 (2007).

[20] F. Zappa, S. Tisa, A. T. and Cova, S., "Principles and features of single-photon avalanche diode arrays," *Actuators A Phys.* **140**, 103–112 (2007).

[21] Hume, D. B., Rosenband, T., and Wineland, D. J., "High-fidelity adaptive qubit detection through repetitive quantum nondemolition measurements," *Phys. Rev. Lett.* **99**, 120502 (Sep 2007).

[22] Stuart, J., Panock, R., Bruzewicz, C., Sedlacek, J., McConnell, R., Chuang, I., Sage, J., and Chiaverini, J., "Chip-integrated voltage sources for control of trapped ions," *Phys. Rev. Applied* **11**, 024010 (Feb 2019).

[23] Stanfield, P. R., Leenheer, A. J., Michael, C. P., Sims, R., and Eichenfield, M., "Cmos-compatible, piezo-optomechanically tunable photonics for visible wavelengths and cryogenic temperatures," *Opt. Express* **27**, 28588–28605 (Sep 2019).

[24] Nielsen, E., Gamble, J. K., Rudinger, K., Scholten, T., Young, K., , and Blume-Kohout, R. *Quantum* **5**, 557 (2021).